# How roughness controls the water repellency of woven fabrics

Alain M. Jonas [a],[*], Ronggang Cai [a], Romain Vermeyen [a], Bernard Nysten [a], Myriam Vanneste [b], David De Smet [b], Karine Glinel [a]

[a] Institute of Condensed Matter and Nanosciences, Université catholique de Louvain, Louvain-la-Neuve, Belgium
[b] Centexbel, Zwijnaarde, Belgium

## HIGHLIGHTS

- A new mathematical analysis of the roughness of fabrics is proposed, including application to experimental profilometry data.
- The model correlates the roughness of woven fabrics with their water repellency when coated by hydrophobic formulations.
- Experiments confirm the correlation between fabric roughness and water repellency.
- The most significant requirements which coatings need to meet to improve the water repellency of fabrics are identified.

## GRAPHICAL ABSTRACT
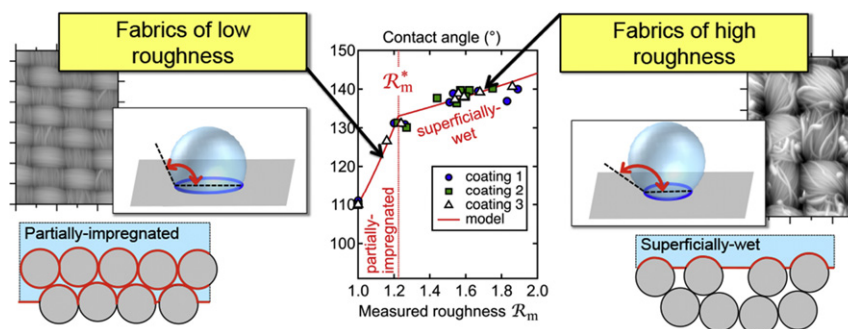
## ABSTRACT

The coming ban on substances of high environmental concern used to provide water repellency to fabrics creates new challenges for the textile industry. Here we show that the design of the texture of woven fabrics is an important parameter to play with in order to achieve higher water repellency, which could help relax the limitations set by more environmentally-friendly coating materials. A mathematical framework is first developed to describe the roughness of woven fabrics and its relationship with water repellency, and metrological aspects of the characterization of the roughness of such fabrics by profilometry are discussed. The roughness of eight different fabric surfaces is then characterized, together with their water repellency after having been coated by wax-based, silicone-based or perfluorobutyl-based commercial polymer formulations. Fabrics of measured roughness lower than a critical value are in a partially-wet state with a substantial pinning of the droplets on their surface and an absence of roll-off whatever the type of hydrophobic coating. Above this critical value, the fabrics enter the superficially-wet state, in which the contact angle becomes controlled by the amount of air trapped in the texture. In this regime, the roll-off angle strongly depends on the wetting hysteresis of the coating material.

## 1. Introduction

Fabrics designed for outdoor use need to be water-repellent, which is typically achieved by coating them with a thin hydrophobic polymer layer. Until recently, polymers with long perfluoroalkyl chains were used for that purpose, owing to the strong hydrophobicity of perfluoroalkanes; additionally, the good oleophobicity of these compounds also results in anti-soiling/anti-staining properties [1]. However, the environmental persistence of bio-accumulative long perfluoroalkyl chains [2] has led to stringent regulatory restrictions on their use [3,4]; similar banning measures are also anticipated for shorter perfluoroalkyl chains [5]. As a consequence, textile producers

are switching to other types of hydrophobic coatings, based on silicone rubber or alkyl chains (waxes), often with a moderate loss of properties.

However, the water repellency of a fabric does not only depend on the chemical composition of its outer surface, but also on its texture which controls its roughness and the amount of air trapped in the fabric when in contact with water. Fabrics are inherently rough due to the weave pattern of the yarns and the packing of textile fibers in the yarns. It might thus reasonably be assumed that proper weaving strategies, associated to a proper selection of yarns, might also significantly contribute to the improvement of water repellency. This however requires to develop a deep understanding of the link between fabric texture and water repellency, which is the aim of this article. Although many excellent previous studies exist on the wetting of rough surfaces [6–18], theoretical studies on common woven fabrics are scarcer [13,15,19,20,21], even though they are important daily-life materials facing critical environmental challenges.

By varying the distance between the filaments in the yarns and their diameter, or by nanostructuring the fiber surfaces, extremely efficient superomniphobic surfaces could be obtained, as recently reviewed [22]; geometric considerations based either on mesh models [13,15,20] or on the recursiveness of hierarchical fabric structures [21] were able to predict wetting by a range of fluids. However, these studies rest on simplified models of fabric texture, and invariably use fluorinated compounds as fabric coatings, which does unfortunately not comply with coming environmental regulations.

Here we show that the water repellency of woven fabrics can be parametrized by their experimentally-measured roughness, and we provide a series of mathematical tools for the prediction of wetting properties from measured maps of the local roughness of fabrics. Water repellency is characterized by the contact angle of a water droplet on the fabric, $\theta$, and its roll-off angle, $\theta_{\mathrm{ro}}$. Six polyester fabrics are studied, displaying plain weave patterns with identical bottom and top sides, together with one fabric with a twill weave and therefore two different sides, resulting in eight different fabric surfaces (Fig. 1 and Table S1 in the Supplementary Information). These fabrics are coated either by a perfluorobutyl modified-polyurethane aqueous formulation, by a silicone rubber aqueous suspension, or by a wax/melamine resin aqueous dispersion (Table 1).

The focus of the work is on providing a mathematical analysis and experimental characterization of the roughness of woven fabrics, and on elucidating the basic relationships between measured roughness and water repellency depending on the type of coating, for the case of woven fabrics. Chemical compositions of the coating formulations and weaving processes are therefore secondary in the analysis. The reader is provided with new mathematical and experimental tools to analyze the roughness of woven fabrics; additionally, water repellency is demonstrated to strongly depend on the proper choice of fabric microstructure.

## 2. Methods

### 2.1. Materials and coating deposition

The fabric samples were polyester fabrics provided by textile manufacturers. The commercial coating materials were obtained from the companies mentioned in Table 1. The PDMS formulation is a finely-dispersed water-based silicone emulsion containing 17 wt. % percent of solid. The size of the particles in this suspension is in the nanometer range. The C4F formulation is a water-based emulsion containing a fluoropolymer (polyurethane grafted with perfluorobutyl chains) containing 30 wt. % of solid. The wax formulation is a dispersion of paraffin oils and a fat-modified melamine resin. The coating procedure was the same for each type of formulation and sample, except for flat samples which were obtained by spin-coating on silicon wafers. The as-obtained PDMS and C4F suspensions were

diluted with Milli-Q water (resistivity 18.2 M$\Omega$·cm, obtained from a Merck Millipore system), to reach a final concentration of 1.5 wt. % solid; the as-received wax formulation was diluted by a factor of 12.5. The fabrics were dip-coated for 3 min in these diluted suspensions, and annealed for 2 min at 150°C on a hot plate to dry them and crosslink the polymer of the coating.

To obtain flat samples by spin-coating on silicon wafers, an undiluted PDMS commercial formulation was used, while the two other commercial formulations were diluted by a factor of 2. Spin-coating was performed at 3000 rpm for 30 s, followed by 2 min annealing at 150°C.

### 2.2. Profilometry measurements

Profilometry was performed with a DektakXT (Bruker), using a stylus with a tip of 0.7 $\mu$m curvature radius scanned at a rate of 286 $\mu$m/s with an applied force of 1 mg, with a sampling resolution of 2 $\mu$m in the $x$-direction and of 0.951 $\mu$m in the $y$-direction. These parameters correspond to our standard conditions leading to the measured roughness $\mathcal{R}_{\mathrm{m}}$; other scanning conditions were sometimes used as mentioned in the text. Each line scan was started from the same reference height obtained by sticking a smooth tape on the fabric, scans being performed in the ' valley mode'. The image size was $1 \times 2$ mm$^2$; after discarding the points corresponding to the reference tape, a typical useful image size is $1 \times 1.5$ mm$^2$.

### 2.3. AFM measurements

Atomic Force Microscopy (AFM) was performed with an ICON Dimension (Bruker). A silicon probe from Nanosensors was used (force constant $\sim$40 N/m, apex radius of curvature $< 7$ nm). Images were acquired in tapping mode at 1 Hz over regions of $3 \times 3$ $\mu$m$^2$.

### 2.4. Contact and roll-off angle measurements

These measurements were performed on an OCA 20 goniometer from Dataphysics with water droplets of 10 $\mu$L volume. Contact angle measurements were performed at four randomly-selected positions, and the average value and standard error computed. Due to the fact that the fabric is inherently non-smooth, there is some uncertainty in the definition of the limiting lines representing the ideal interface between the fabric and the testing liquid. Roll-off angle measurements were performed by depositing the water droplet on the horizontal fabric, followed by progressive tilting until the droplet rolls-off. For the measurement of advancing and receding contact angles on flat samples, an initial water droplet of 5 $\mu$L volume was dispensed onto the surface with the needle positioned inside the droplet. Then, 2.5 $\mu$L of water was progressively added until the contact angle reached a constant value which was recorded as the advancing contact angle. Then, 2.5 $\mu$L of water was progressively removed until the contact angle reached another constant value noted as the receding contact angle.

### 2.5. Mathematical treatment of the images

All operations were performed with home-written routines developed in Wavemetrics Igor Pro. The profilometry images $h(x,y)$ were made horizontal by subtraction of a tilted plane. The local roughness $\rho(x,y)$ was obtained by numerical differentiation and Eq. (11); points for which $|\partial h/\partial x|$ or $|\partial h/\partial y| \geq 6$ were discarded since they correspond to glitches. The roughness is the average of $\rho$ on the image. The correlation functions were computed by Fourier-transforming the images and back Fourier-transforming the square of the magnitude of the Fourier transforms. AFM images were treated similarly, except for a flattening operation with a bidimensional polynomial function to remove the curvature due to the fibers.
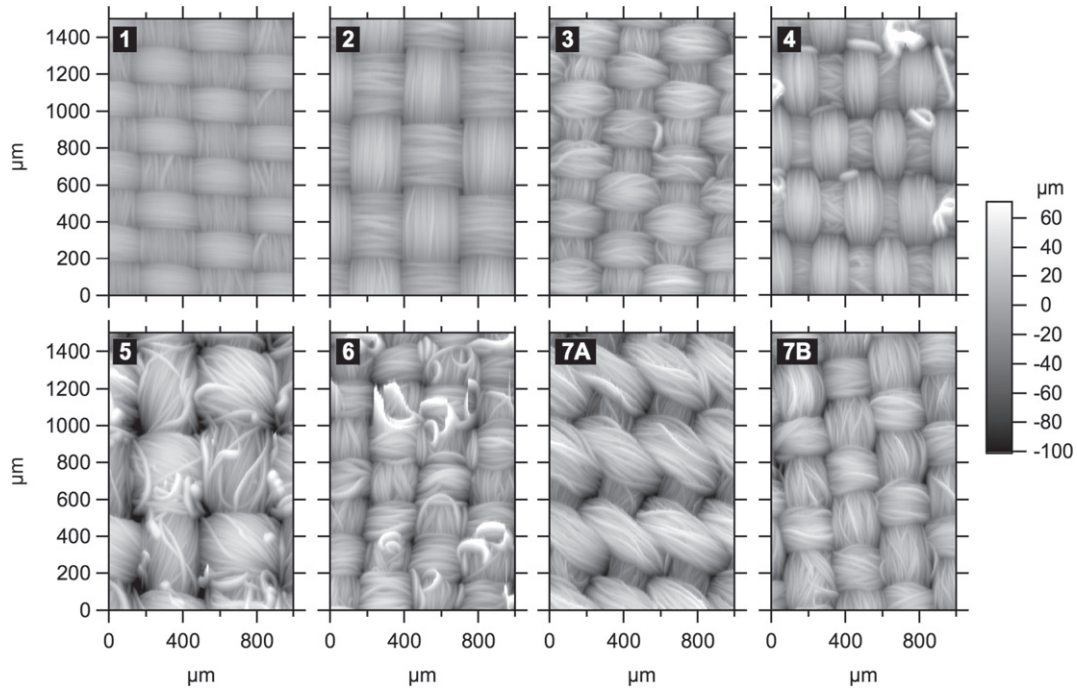
**Fig. 1.** Profilometry topography images of the fabrics used in this study, with sample numbering. Sample 7 is a twill weave with consequently two different sides noted A and B.

## 3. Results and discussion

### 3.1. Roughness of a hydrophobic woven fabric: theoretical aspects

#### 3.1.1. Wetting states and contact angle equations

When in contact with water, a hydrophobic fabric may be in one of an ensemble of partially-impregnated states, in which water partially penetrates the top of the fabric (Fig. 2a); or in the superficially-wet state, in which water only rests over a limited fraction of the hemicylindrical upper part of the top textile fibers (Fig. 2b). For protection against water, the superficially-wet state is desired. Fabrics of very low roughness tend to be in a partially-impregnated state whereas, for higher roughness, trapping of air in the topmost cavities of the fabric leads to the superficially-wet state.

At the droplet scale, the macroscopic contact angle of a water droplet on the fabric, $\theta$, is determined by an equilibrium of forces at the vicinity of the triple line, over a peripheral ring of vanishing width $\epsilon$ and area $A = 2\pi R\epsilon$ where $R$ is the radius of the contact patch (inset of Fig. 2). At the fiber scale, the Young-Dupré's equation applies, with the water/air interface making a local contact angle $\theta_0$ with the tangent to the fiber at the triple line (Fig. 2). Of note, the Young-Dupré's equation is only valid for smooth, isotropic and homogeneous solids inert to the probe fluid [24], which is the

case here at the sub-fiber scale; it also supposes thermodynamic equilibrium.

Due to the roughness, the area $A_c$ of the composite interface (red lines in Fig. 2) is larger than the projected area $A$ of the peripheral ring by a factor thereafter called the *composite roughness* $\mathcal{R}_c$:

$$\mathcal{R}_c \triangleq \frac{A_c}{A}. \tag{1}$$

The composite interface comprises wetted fibers and air, with the surface fraction of wet solid being $\phi$. The effective area of wet solid is thus $\phi A_c$ and the one of water/air contact is $(1 - \phi)A_c$. With these definitions, it is demonstrated in Section 1 of the Supplementary Information, using an argument inspired from previous work [12], that:

$$\cos\theta = \mathcal{R}_c\left(\phi\cos\theta_0 - (1 - \phi)\right). \tag{2}$$

This equation is valid for any partially-impregnated state and the superficially-wet state. However, it is more convenient and consistent with usual conventions to write this equation differently for the case of the superficially-wet state, when the liquid does not

**Table 1**
Characteristics of the hydrophobic coatings used to modify the fabrics.

| Coating type | Commercial name | Short name | $\theta_0(a,b)$ (°) | $\theta_{0a}^{(a,c)}$ (°) | $\theta_{0r}^{(a,d)}$ (°) | $\mu^{(e)}$ (N/m) | $\mu^{(f)}$ (N/m) |
|---|---|---|---|---|---|---|---|
| Wax-modified melamin resin | Schoeller Protec FF | wax | 110 | 110 | 91 | 0.024 | 0.043 |
| Silicone rubber | Wacker® HC303 | PDMS | 111 | 108 | 85 | 0.029 | 0.065 |
| Perfluorobutyl-modified polyurethane | 3M™ PM900 | C4F | 110 | 116 | 42 | 0.086 | 0.090 |

(a) Standard error on contact angles is *ca.* 1°;
(b) Contact angle measured over a flat spincoated film;
(c) Advancing angle measured over a flat spincoated film;
(d) Receding contact angle measured over a flat spincoated film;
(e) Pinning parameter computed from Eq. (7) using $\gamma = 72.86 \times 10^{-3}$ J/m² [23].
(f) Pinning parameter computed from the fits of the contact and roll-off angles.
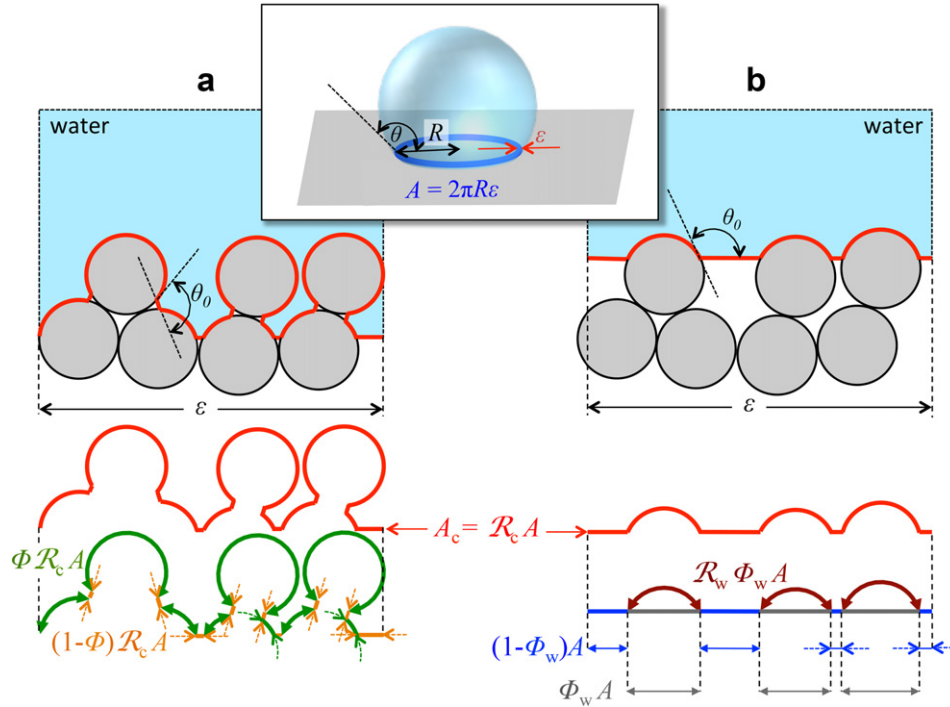
**Fig. 2.** Schematic transverse cuts of a woven fabric made of hydrophobic cylindrical fibers (a) in one among many possible partially-impregnated states and (b) in the superficially-wet state, with $\theta_0 > \pi/2$ the contact angle of water over a flat surface of identical chemical composition. The inset is the geometry of the macroscopic droplet, showing the macroscopic contact angle $\theta$ and the peripheral ring of projected area $A = 2\pi R\varepsilon$. The thick red lines in panels a and b are the composite interfaces, of developed area $A_c = \mathcal{R}_c A$; the wet fraction of the composite interface is $\phi$ (green line in panel a). In the case of the superficially-wet state (panel b), it is more convenient to define the projected fraction of wet solid $\phi_w$ (grey lines) and the roughness of this fraction $\mathcal{R}_w$ (brown line).

penetrate the cavities present at the top surface of the fabric. The *projected* fraction of wet solid, $\phi_w$, is defined as the ratio between the *projected* area of wet solid at the composite interface and the total projected area, $A$ (Fig. 2b). The *wet roughness* $\mathcal{R}_w$ is defined as the ratio of the actual area of the wet solid relative to its projected area. It can be shown that:

$$\phi = \frac{\mathcal{R}_w}{\mathcal{R}_c}\phi_w \quad \text{and}$$
$$\mathcal{R}_c = \mathcal{R}_w\phi_w + 1 - \phi_w \text{(superficially-wet state);} \tag{3}$$

therefore, Eq. (2) becomes:

$$\cos\theta = \mathcal{R}_w\phi_w\cos\theta_0 - (1 - \phi_w), \tag{4}$$

which is the well-known Cassie-Baxter equation including a correction factor $\mathcal{R}_w$ for the roughness of the solid/water interface [16]. One should not confuse $\phi$ and $\phi_w$, which are defined by the real and projected areas of the wet fraction of the composite interface, respectively. Likewise, $\mathcal{R}_c$ is very different from $\mathcal{R}_w$ as shown in Fig. 2.

### 3.1.2. Equation for the water roll-off angle

Consider now a droplet resting over an initially-horizontal fabric, which is progressively tilted away from horizontality. At some roll-off angle $\theta_{ro}$, the droplet will start moving over the fabric. For droplets of circular contact patch moving on flat surfaces, it was demonstrated that [25,26]:

$$m_V g V \sin\theta_{ro} = 2R\gamma(\cos\theta_{0r} - \cos\theta_{0a}), \tag{5}$$

in which $g$ is the acceleration due to gravity, $m_V$ the mass per unit volume of water, $V$ the volume of the droplet, $\gamma$ the surface tension

of water, and $\theta_{0r}$ and $\theta_{0a}$ the receding and advancing contact angles of water on the flat surface, respectively. This equation equates the gravitational pull and the friction force experienced by the droplet just when it starts moving. In agreement with a suggestion by Varanasi et al. [27], this equation can be adapted to the case of a rough surface by taking into account the fraction of water/solid contact interface, which modulates the friction force:

$$m_V g V \sin\theta_{ro} = 2R\phi\mathcal{R}_c\gamma(\cos\theta_{0r} - \cos\theta_{0a}). \tag{6}$$

For the specific case of the superficially-wet state, one can replace $\phi\mathcal{R}_c$ by $\mathcal{R}_w\phi_w$ according to Eq. (3). Defining a pinning parameter $\mu$ (N/m) by[1]:

$$\mu = \gamma(\cos\theta_{0r} - \cos\theta_{0a}), \tag{7}$$

Eq. (5) transforms into:

$$m_V g V \sin\theta_{ro} = 2R\phi\mathcal{R}_c\mu, \tag{8}$$

from which the radius $R$ of the contact patch can be eliminated since, for a spherical cap, it is related to the contact angle $\theta$ by [11]:

$$R = \sin\theta\left(\frac{3V}{\pi(2 - 3\cos\theta + \cos^3\theta)}\right)^{\frac{1}{3}}. \tag{9}$$

---

[1] The definition of the pinning parameter by Varanasi et al. differs from ours by a factor 1/2; additionally, the r.h.s. of their equivalent to Eq. (6) is a factor of $\pi/2$ larger than in the present work, due to a different evaluation of the work done by the moving droplet.

The pinning parameter of water on the material of the fabric encapsulates the dynamical aspects of the water/solid interaction on a flat surface; it is associated to reorganization of the water/solid interface upon wetting and dewetting.

### 3.1.3. Ideal experimental roughness

Take a fabric lying flat in the horizontal $(x, y)$ plane. Define the local variable $h(x, y)$ as the height of the top external surface of the fabric, that would be measured when scanned by an infinitely-sharp tip of zero radius of curvature. This ideal tip cannot probe regions below overhangs; in particular, for a fabric made of cylindrical fibers, it cannot obtain information on the bottom hemicylindrical part of the fibers. This definition is thus most suited to fabrics in the superficially-wet state, in which water does not probe the lower hemicylindrical part of the fibers (Fig. 2b). Note that this definition of $h(x, y)$ would also be convenient for any non-reentrant surface coated by a hydrophobic layer.

When the ideal tip is scanned over a surface $A$ of the horizontal plane, the effectively-probed area, $A_\sim$, is larger than the projected area, $A$, by a factor $\mathcal{R}_A \geq 1$ thereafter called the *ideal roughness measured over A*. It is well-known that [28]:

$$\mathcal{R}_A \triangleq \frac{A_\sim}{A} = \frac{1}{A} \int_A \sqrt{1 + \left(\frac{\partial h}{\partial x}\right)^2 + \left(\frac{\partial h}{\partial y}\right)^2} \, dx \, dy. \tag{10}$$

It is convenient to define the function $\rho(x, y)$, hereafter called the *local roughness* of the fabric:

$$\rho(x, y) \triangleq \sqrt{1 + \left(\frac{\partial h}{\partial x}\right)^2 + \left(\frac{\partial h}{\partial y}\right)^2}; \tag{11}$$

with this definition, the ideal roughness measured over $A$ (Eq. (10)) is simply the average of the local roughness over $A$:

$$\mathcal{R}_A = \langle \rho \rangle_A. \tag{12}$$

### 3.1.4. Distribution of ideal roughness and minimal image size for roughness measurement

When the ideal roughness is measured over an ensemble of regions of identical area $A$, different values of roughness $\mathcal{R}_A$ will generally be obtained. Due to the linearity of the averaging operation, the average of these values is (Section 2, Supplementary Information):

$$\langle \mathcal{R}_A \rangle = \mathcal{R}, \tag{13}$$

in which

$$\mathcal{R} \triangleq \lim_{A \to \infty} \frac{1}{A} \int \rho(x, y) \, dx \, dy \tag{14}$$

is the ideal roughness measured over an infinitely-large fabric sample, thereafter called *total ideal roughness*. Consequently, the average contact angle does not depend on the size of the probing droplet either, provided enough droplets are measured.

It is also possible to compute the variance $\sigma_A^2$ of the distribution of ideal roughness when measured over domains of area $A$. As demonstrated in Section 2 of the Supplementary Information,

$$\sigma_A^2 = \int \mathcal{C}_2(x, y) \tilde{\mathcal{A}}(x, y) \, dx \, dy - \mathcal{R}^2, \tag{15}$$

in which

$$\mathcal{C}_2(x, y) \triangleq \lim_{S \to \infty} \frac{1}{S} \int_{(u,v) \in \mathcal{S}} \rho(u + x, v + y) \rho(u, v) \, du \, dv \tag{16}$$

is the (bidimensional) auto-correlation function of the local roughness and $\tilde{\mathcal{A}}(x, y)$ is proportional to the auto-correlation of the shape of the domains. Eqs. (13) and (15) are general and not limited to the case of fabrics.

For square domains of lateral side $a$, Eq. (15) becomes:

$$\sigma_A^2 = \frac{2}{a^2} \int_{x=0}^{a} \int_{y=-a}^{a} u(x, y) \, \mathcal{C}_2(x, y) \, dy \, dx - \mathcal{R}^2, \tag{17}$$

with $u(x, y) = (1 - x/a)(1 - |y|/a)$. This equation is useful to determine the minimal image size from which $\mathcal{R}_A$ will be close to the large-scale value $\mathcal{R}$ (i.e., the total ideal roughness). Indeed, $\mathcal{C}_2(x, y)$ is a globally-decreasing function of $(x, y)$, starting at $\mathcal{C}_2(0, 0) = \langle \rho^2 \rangle$ and tending towards $\langle \rho \rangle^2$ when either $x$ or $y \to \infty$; therefore, $\sigma_A^2$ is also a globally-decreasing function of $a$, with

$$\lim_{a \to 0} \sigma_A^2 = \langle \rho^2 \rangle - \langle \rho \rangle^2 \text{ and } \lim_{a \to \infty} \sigma_A^2 = 0. \tag{18}$$

To obtain a value of roughness close to the total ideal roughness, the image size should be selected to ensure that $\sigma_A^2$ be close to zero.

### 3.1.5. Relationship between total ideal roughness, and wet or composite roughnesses

The total ideal roughness $\mathcal{R}$ is not identical to the roughness effectively probed by a droplet of water as depicted in Fig. 2. Indeed, in the superficially-wet state (Fig. 2b), only a fraction of $\mathcal{R}$ contributes to the wet roughness $\mathcal{R}_w$; whereas in partially-impregnated states (Fig. 2a), the composite roughness $\mathcal{R}_c$ may be much larger than $\mathcal{R}$. More precisely, it is shown in Section 3 of the Supplementary information that, in the superficially-wet state, the wet roughness tends to a constant value independent of the actual roughness of the fabric:

$$\mathcal{R}_w \to \frac{\pi - \theta_0}{\sin \theta_0} \text{(superficially-wet state)}; \tag{19}$$

for a contact angle $\theta_0 = 110°$ as in the present study, $\mathcal{R}_w \to 1.3$.

It is not possible to derive a similarly-general equation for the case of a partially-impregnated state. However, one can generally write that:

$$\mathcal{R}_c = F(\mathcal{R}, \theta_0), \tag{20}$$

in which $F$ is an unknown function. As will be shown later, the partially-impregnated state only exists for relatively low values of total ideal roughness ($\mathcal{R} \leq\sim 1.2$). Therefore, Eq. (20) can be developed to first order around $\mathcal{R} = 1$, leading to:

$$\mathcal{R}_c \approx 1 + a_{\theta_0} (\mathcal{R} - 1) \text{(partially-impregnated state)}, \tag{21}$$

in which $a_{\theta_0}$ only depends on $\theta_0$; for the coatings of the present study which have almost the same $\theta_0$ value, $a_{\theta_0}$ is a constant. Likewise, since $\phi \to 1$ for a partially-impregnated state,

$$\phi \approx 1 + b_{\theta_0} (\mathcal{R} - 1) \text{(partially-impregnated state)}. \tag{22}$$

However, one should be aware that different partially-impregnated states will have different values of $a_{\theta_0}$ and $b_{\theta_0}$.

### 3.1.6. Minimal droplet size for contact angle measurements

Eq. (15) can also be used to determine the minimal droplet size above which a single measurement of the contact angle will converge towards its large-scale value. As mentioned before, for a droplet of circular symmetry with a triple line of radius $R$, the relevant area

of contact at the vicinity of the triple line is a ring of central radius $R$ and of vanishing width $\epsilon$. Importantly, the relevant roughness is not measured over the area of the disk enclosed by the triple line, as sometimes erroneously thought; indeed, the equilibrium shape of a droplet does not depend on the nature of the surface away from the triple line. In this case, as demonstrated in Section 2 of the Supplementary Information,

$$\sigma_R^2 \triangleq \sigma_{A=(2\pi R\epsilon \to 0)}^2 = \frac{2}{\pi} \int_0^{\pi/2} \mathcal{C} \left(2R \sin \theta\right) \ \mathrm{d}\theta - \mathcal{R}^2, \tag{23}$$

in which the one-dimensional radial correlation function $\mathcal{C}$ is defined as the circular average of the correlation function $\mathcal{C}_2$:

$$\mathcal{C}(r) \triangleq \frac{1}{2\pi} \int_0^{2\pi} \mathcal{C}_2 \left(r \cos \omega, r \sin \omega\right) \ \mathrm{d}\omega, \tag{24}$$

where $(r, \omega)$ designate polar coordinates. Although the droplet shape is determined by the wet or composite roughness and not the total ideal roughness, Eq. (23) can still be applied because the lateral correlation functions of these differently-defined roughnesses should be similar.

### 3.1.7. Fraction of wet fabric in the superficially-wet state

In the superficially-wet state, the relevant roughness appearing in the wetting Eq. (4) is the roughness $\mathcal{R}_w$ measured over the wet part of the fabric on the peripheral ring of the droplet. It is possible to have access from maps of the local roughness $\rho(x, y)$ to estimates of $\mathcal{R}_w$ and of the projected fraction of wet solid $\phi_w$ for a given fabric in the superficially-wet state. As demonstrated in Section 3 of the Supplementary Information, an estimate for the projected fraction of wet solid is the fraction of the fabric for which the following two conditions are simultaneously met:

$$\rho(x, y) \leq -\frac{1}{\cos \theta_0} \text{ and } H(x, y) \leq 0, \tag{25}$$

in which $H(x, y)$ is the local mean curvature of the surface. These conditions were obtained for fabrics made of cylindrical fibers, but are similar to conditions proposed for more general cases [11,12]. Importantly, these conditions define the wet regions in the superficially-wet state only; they do not apply to the partially-impregnated states given the way $h(x, y)$ is defined.

The wet roughness $\mathcal{R}_w$ in this state is the roughness measured only over the wet regions respecting conditions (25). It can be directly measured on maps of $\rho(x, y)$, and should converge towards the constant value given by Eq. (19).

### 3.1.8. Roughness due to the fiber packing in the yarns, $\mathcal{R}_y$, and due to the weave pattern of the yarns, $\mathcal{R}_w$

It is interesting to identify which one among either the weave pattern of the yarns, or the fiber packing in the yarns, is the stronger contributor to the roughness. Section 4 of the Supplementary Information shows how height images can be separated in two component images:

$$h(x, y) = h_y(x, y) + h_w(x, y), \tag{26}$$

in which $h_y(x, y)$ mainly contains the fluctuations of height arising from the packing of the fibers in the yarns, and $h_w(x, y)$ the fluctuations of height resulting from the weave pattern of the yarns. An example of decomposition is given in Fig. 3 for sample 7A. The decomposition procedure involves low-pass filtering of the image to extract the weave pattern only.

It is demonstrated in Section 4 of the Supplementary Information that

$$\mathcal{R} \approx \mathcal{R}_y + \mathcal{R}_w - 1, \tag{27}$$

which indicates that the roughness of the fabric is related to the sum of the roughnesses of the fiber packing in the yarns and of the weave pattern of the yarns. The approximation is only valid when the roughness of the weave pattern is small enough; however, it applies to other types of surfaces than fabrics, when one component of the roughness is a small contributor to the total roughness.

### 3.2. Roughness of a fabric: metrological aspects

Height images can be obtained by profilometry and atomic force microscopy (AFM). Whereas the former permits scanning large areas, its lateral resolution is typically limited to ca. 1 $\mu m$. In contrast, AFM provides access to images of increased lateral resolution, in the nm scale, but is limited to small fields of view. Profilometers can typically
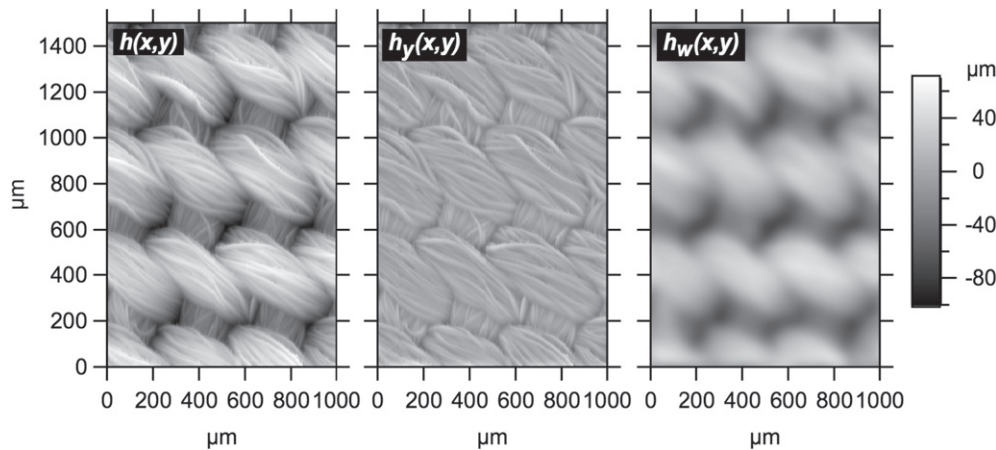


**Fig. 3.** Decomposition of the height profile $h(x, y)$ into a height fluctuation due to the packing of the fibers in the yarns, $h_y(x, y)$, and a height fluctuation due to the weave pattern of the yarns, $h_w(x, y)$. The decomposition was performed for sample 7A using the methodology described in Section 4 of the Supplementary Information, using a Gaussian low pass filter of 25 $\mu m$ standard deviation.

be based on optical measurements, or monitor the vertical displacement of a stylus scanned over the surface (as in AFM). Attempts performed with optical profilometers proved to be disappointing, due to strong pixel-to-pixel shot noise requiring strong smoothing before differentiation to obtain the local roughness by Eq. (11). In contrast, stylus profilometry was much more effective in obtaining noise-free images, provided each successive line scan started from a flat reference surface (see Experimental Section for details). The few remaining glitches due to loose loops or dangling fibers were generally limited in number and therefore did not influence the average of the local roughness. Repeated measurements performed on the same sample at the same location indicated the roughness to be repeatable within *ca.* 0.01. However, differences are larger for measurements performed at different locations of the same fabric (*ca.* 0.1), due to the intrinsic variability of the fabrics; this is especially true for rougher samples exhibiting loose loops and dangling fibers, such as samples 5–7.

Both stylus profilometry and AFM provide images that have systematic errors due to finite sampling and dilation by the tip shape, and dynamic effects due to the limitations of the feedback loop which controls the vertical motion of the tip. As a result, these techniques only provide an approximation $h_m(x, y)$ of the ideal image $h(x, y)$, giving rise to a *measured roughness* $\mathcal{R}_m$ which is generally lower than the ideal roughness $\mathcal{R}$.

### 3.2.1. Rate effects in stylus profilometry

The scanning speed of the stylus determines the sampling resolution as well as the capability of the feedback loop to follow rapid variations of height. Fig. S4 of the Supplementary Information displays a set of images obtained at different scanning speeds for fabric sample 7A, showing that the details of the fibers scanned perpendicularly by the tip become sharper at lower speeds. The measured roughness is plotted versus scanning speed in Fig. 4 for three representative fabrics of this study; the increase of measured roughness as speed decreases is obvious.

These data can be extrapolated towards zero scanning rate to obtain the zero-rate roughness $\mathcal{R}_m^\circ$. Measurements at small scanning rates are however impractical because they require extremely long acquisition times (more than 15 h for the slowest scan rate of this study), which results in drifts. Therefore, the measurements have generally been performed at the more practical scanning rate of *ca.* 286 $\mu$m/s, corresponding to an acquisition time of *ca.* 1 h per image; this is the case, *e.g.*, for the images of Fig. 1. The roughness obtained at this standard rate, $\mathcal{R}_m^s$, allows us to compare and sort samples by increasing roughness. When more absolute values of roughness are needed, the data of Fig. 4 indicate that:

$$\mathcal{R}_m^\circ - 1 \simeq 1.7(\mathcal{R}_m^s - 1). \tag{28}$$

For practicality, in the sequel the roughness measured at the standard rate will be simply designated as $\mathcal{R}_m$ instead as $\mathcal{R}_m^s$.

### 3.2.2. Limited lateral resolution of stylus profilometry

Additionally, the tip of the stylus of the profilometer has a finite radius of curvature (0.7 $\mu$m in this work), which prevents to obtain information on protuberances and cavities smaller than *ca.* 1 $\mu$m. Therefore, complementary atomic force microscopy (AFM) images were obtained over small 3 × 3 $\mu$m$^2$ regions, significantly smaller than the fiber diameter of the fabrics. After polynomial flattening to remove the deformation due to fiber curvature, the measured AFM roughness $\mathcal{R}_{AFM}$ can be computed. If the nanometer-scale roughness of the fiber surface is statistically independent from the micrometer-scale roughness created by the fibers of the fabric:

$$\mathcal{R}_m = \mathcal{R}_{AFM} \mathcal{R}_{prof} \quad , \tag{29}$$
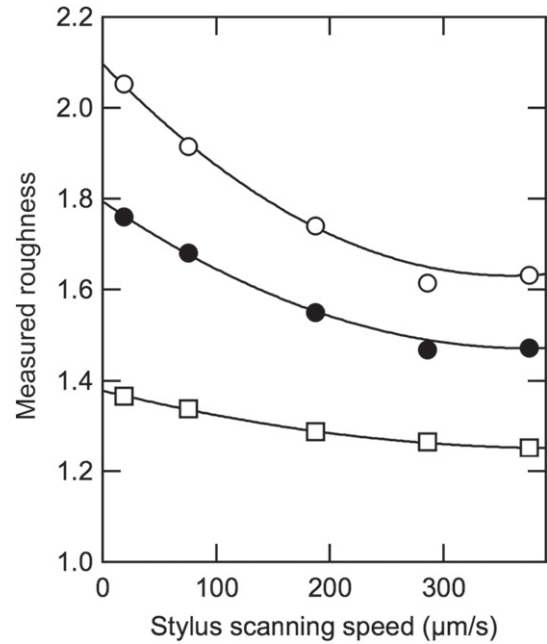


**Fig. 4.** Variation of the roughness measured by stylus profilometry depending on the scanning rate of the stylus for, from bottom to top, fabric samples 2, 4 and 7A. The continuous curves are polynomial fits.

in which $\mathcal{R}_{prof}$ is the roughness from the profilometry images. In this study, $\mathcal{R}_{AFM}$ was always close to 1 (within 1%), indicating that, for all the fabrics of this study, be them coated or not, the nanoscale roughness is entirely negligible (results not shown). Therefore, profilometry images contain all the relevant information.

### 3.3. Experimental measurements on non-coated fabrics

The profilometry images $h(x, y)$ of the eight fabric surfaces obtained at the standard scanning rate are displayed in Fig. 1. Some fabrics exhibit the presence of loose or dangling fibers, which were sometimes not imaged properly by the stylus of the profilometer (*e.g.*, for sample 6); however, the affected pixels were limited in number and could be removed from further computations. The diameter of the textile fibers is between 10 and 25 $\mu$m and is sometimes different for warp and weft yarns; the dimensions of the smallest unit cell of the weave patterns are comprised between 0.3 and 0.8 mm (Table S1).

Maps of the local roughness $\rho(x, y)$ were then computed from the height images using Eq. (11) (Fig. 5), from which the fabric roughness measured at the standard rate, $\mathcal{R}_m$, was obtained by Eq. (12). The measured roughness ranges from 1.19 to 1.77 (Table S1), confirming that the weave pattern and yarn type may indeed result in significantly different values of roughness. The maps of local roughness clearly show that the edge of fibers and yarns, as well as dangling fibers, dominantly contribute to the roughness, which is expected since the local roughness depends on the spatial derivatives of $h$ which are higher close to edges.

### 3.3.1. Roughness from fiber-in-yarn packing and from weave pattern

The images of all non-coated fabric samples were decomposed in two contributions according to Eq. (26), providing access to the measured roughness arising from the fiber packing in the yarns, $\mathcal{R}_y$, and from the weave pattern of the yarns, $\mathcal{R}_w$. The results are displayed in Fig. 6, showing that the contribution from the weave pattern is much smaller than the one from the fiber packing in the yarns. This is because the lateral scale of the fluctuations of height is much larger
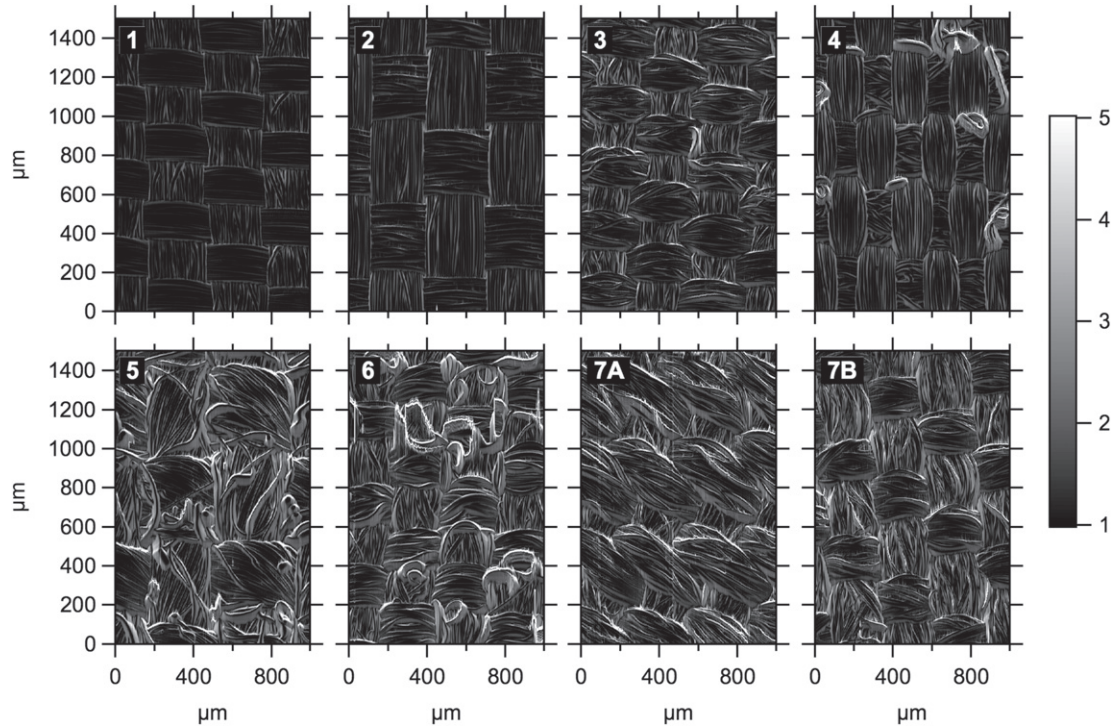
**Fig. 5.** Maps of the local roughness $\rho(x,y)$ (Eq. (11)) for the eight fabric surfaces of this study, computed from the stylus profilometry images of Fig. 1.

for the weave pattern, resulting in smaller spatial derivatives of $h_w$ compared to $h_y$. The open circles in Fig. 6 also show that, for all the samples of this study,

$$\mathcal{R} \approx \mathcal{R}_y + \mathcal{R}_w - 1, \tag{30}$$

an approximation demonstrated in Section 4 of the Supplementary Information.

### 3.3.2. Minimal size for meaningful measurements

Given the hierarchical lateral texture of a fabric surface, the question arises as to what is the size from which the measured roughness converges towards a constant value. A related question is the size from which a droplet feels a constant roughness. As explained in the theoretical section, these questions can be answered by computing the correlation functions of the local roughness, from which the variances of the distribution of roughness measured either over square images of lateral size $a$ ($\sigma_A^2$) or by droplets of contact radius $R$ ($\sigma_R^2$) can be obtained by Eqs. (17) and (23), respectively.

The correlation functions for all non-coated fabrics are displayed in section 6 of the Supplementary Information; they exhibit a strong central peak resulting from fiber-to-fiber correlation, which vanishes over $200\,\mu m$, with weaker peaks in the $200–800\,\mu m$ range arising from yarn-to-yarn correlation. The variances $\sigma_A^2$ and $\sigma_R^2$ computed from these correlation functions are displayed in Fig. S6; the variance decreases more or less rapidly with size depending on sample, rougher samples generally needing larger sizes to reach a constant variance. For image sizes $a \geq \sim 600\,\mu m$ or droplets of radius $R \geq \sim 300\,\mu m$, the variances are close to constant; these limits essentially correspond to the size of the unit cells of the fabrics (Table S1). The profilometry images of Fig. 1 are therefore large enough to obtain the total roughness $\mathcal{R}$. This also proves that droplets of radius above $ca.\ 300\,\mu m$ (volume larger than $ca.\ 120\,nL$) are already large enough to provide an accurate average of surface properties. Conversely, smaller droplets may feel widely different surface properties, and therefore should exhibit a range of contact angles – this might be

important when comparing the behavior of a fabric in a drizzle or a normal rain.

### 3.4. Wetting properties of coated fabrics

The static, advancing and receding contact angles of the three types of commercial coatings were measured over flat thin films obtained by spincoating the formulations on silicon wafers, followed by drying/curing for 2 min at $150°C$. The roughness of these samples was measured by AFM and found to be 1.00 (images not shown). The three coatings have identical values of static contact angle ($110–111°$) but their advancing and receding contact angles differ substantially, leading to strongly different values of pinning parameter $\mu$ as well (Table 1). Scanning electron microscopy (SEM) images (Fig. S7) indicated the wax- and PDMS-based films to be featureless, except for adventitious contamination by dirt or rare scratches. The perfluorobutyl-based films however showed the presence of a few but regularly-present height heterogeneities; these were not numerous enough to affect in a significant way the profilometry or AFM roughness, but might contribute to contact angle hysteresis as well.

The fabrics were then coated with the three different hydrophobic formulations, by dip-coating them in aqueous suspensions and drying/curing them at $150°C$. The roughness was measured again by profilometry and was generally marginally different from the value measured on the bare fabrics, except for a few samples (Table S1). As mentioned above, the AFM-scale roughness was not changed by the coating process and remained very close to 1 for all samples (results not shown).

The water contact $\theta$ and roll-off $\theta_{ro}$ angles were then measured (symbols in Fig. 7a and b), and Eqs. (2)/(4) and (8) were simultaneously fit to the contact and roll-off angle data, respectively. The model was parametrized by the measured roughness $\mathcal{R}_m$, and was based on the assumption that, below a critical value of measured roughness $\mathcal{R}_m^*$, the samples are in a partially-impregnated state, while they enter the superficially-wet state above $\mathcal{R}_m^*$. The equations were simultaneously fit to the data obtained for the three types of

coatings, assuming a single value for $\theta_0$ and the same dependence of $\mathcal{R}_c$, $\mathcal{R}_w$, $\phi$ and $\phi_w$ with $\mathcal{R}_m$ for the three coatings, in agreement with the observation that the contact angles of all coated fabric samples fall on a single curve (Fig. 7a).

In the partially-impregnated state, the contact angle was described by Eq. (2), in which the fraction of wet material at the composite interface is:

$$\phi = 1 - p_1(\mathcal{R}_m - 1), \tag{31}$$

while the roughness of the composite interface is:

$$\mathcal{R}_c = 1 + p_2(\mathcal{R}_m - 1), \tag{32}$$

with $p_1$ and $p_2$ two fit parameters. These expressions are direct consequences of Eqs. (21), (22) and (28).

In the superficially-wet state, the contact angle was described by Eq. (4), in which the projected fraction of wet material is:

$$\phi_w = p_3 - p_4(\mathcal{R}_m - \mathcal{R}_m^*), \tag{33}$$

while the roughness of the wet interface is:

$$\mathcal{R}_w = p_5, \tag{34}$$

with again $p_3$, $p_4$ and $p_5$ three fit parameters. Eq. (34) is a direct consequence of Eq. (19); as for the roughness-dependence of $\phi_w$ (Eq. (33)), it is based on a prior evaluation of $\phi_w$ for all fabrics using the conditions (25) (see below). The critical value $\mathcal{R}_m^*$ is found by requesting $\cos\theta$ to be equal for the two states at $\mathcal{R}_m^*$ [9]. The pinning parameters of each type of coating are three additional fit parameters.

The fits (continuous lines in Fig. 7a and b) represent properly the data with $\theta_0 = 110°$, $p_1 = -0.072$, $p_2 = 4.16$, $p_3 = 0.593$, $p_4 = -0.307$, $p_5 = 1.36$, $\mu_{wax} = 0.043$ N/m, $\mu_{PDMS} = 0.065$ N/m
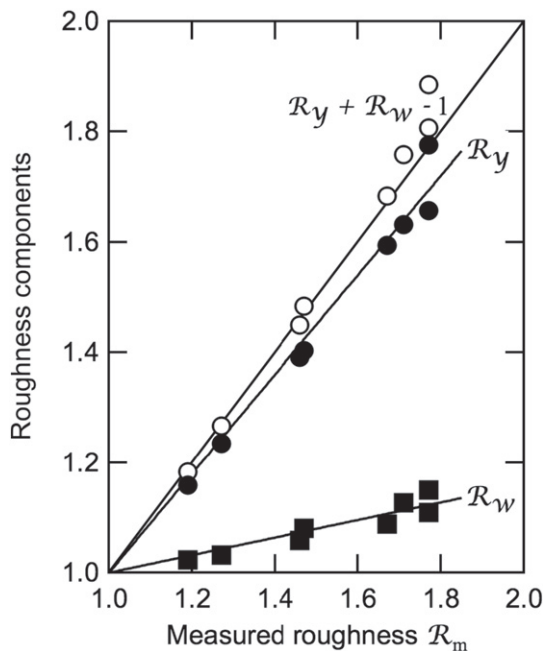


**Fig. 6.** Roughness from the fiber packing in the yarns, $\mathcal{R}_y$ (full circles), and from the weave pattern of the yarns, $\mathcal{R}_w$ (full squares), plotted versus the measured roughness of the profilometry images for all non-coated samples. The weave pattern of the yarns contributes much less to the total fabric roughness. The open circles show that the total roughness is well approximated by $\mathcal{R}_y + \mathcal{R}_w - 1$.

and $\mu_{C4F} = 0.090$ N/m; the agreement is lesser for the roll-off angles due to the larger scatter in the data, indicating that other, secondary factors may also play a role in the rolling-off of water. The critical measured roughness $\mathcal{R}_m^*$ is 1.22 (in our standard acquisition conditions); only sample 1 falls below this threshold (Table S1), all other fabrics thus being in the superficially-wet state.

The value found for $\theta_0$ (110°) is remarkably close to the experimental values measured on flat samples of the three coatings spin-coated over a silicon wafer (110–111°). In contrast, the fitted pinning parameters $\mu$ are higher than the values obtained from the direct measurement of advancing and receding contact angles on flat surfaces (Table 1), but can be sorted in the same order, with the friction force being lower on the wax-based coating, followed by the silicone-based coating, then by the perfluorobutyl-based coating (Table 1). In this work, receding and advancing contact angles were measured by adding and removing water from a static droplet, which considerably differs from the configuration of a rolling droplet; furthermore, additional dynamical factors may also be important to explain the differences between the fitted and measured values of $\mu$. Finally, one cannot exclude small differences of chemical composition of the external surface of the coatings for spincoated flat films and dip-coated fabrics.

The composite roughness $\mathcal{R}_c$ in the partially-impregnated state and the wet roughness $\mathcal{R}_w$ in the superficially-wet state are shown in Fig. 7c. The composite roughness in the partially-impregnated state is substantially larger than the measured roughness, as expected since the profilometer only scans the top roughness of the sample whereas water penetrates deeper in the fabric (Fig. 2a); the wet roughness in the superficially-wet state is 1.36, close to the 1.3 predicted by Eq. (19) when $\theta_0 = 110°$. The fractions of wet solid are shown by the continuous lines in Fig. 7d. As expected, $\phi$ remains close to 1 in the partially-impregnated state, only slightly decreasing with measured roughness. Above the critical roughness, in the superficially-wet state, the projected fraction of wet solid $\phi_w$ decreases faster with roughness. This decrease is actually the main cause for the small increase of the contact angle with roughness in this state.

The projected fraction of wet solid in the superficially-wet state was also directly computed from the profilometry images using conditions (25), assuming either $\theta_0 = 110°$ or $\theta_0 = 120°$ (crosses and circles in Fig. 7d, respectively). The values from the fit to the wetting data (continuous line) are very close to the values directly obtained from the profilometry images when $\theta_0 = 120°$; this slight discrepancy compared to the fitted value of $\theta_0$ (110°) results from the blurring of the details of the image by the profilometer tip, which slightly decreases the slopes of the height profiles. Nevertheless, the good agreement between results obtained independently by the two techniques (wetting data *versus* profilometry) provides a strong support to the present analysis which is close to quantitative.

## 4. Conclusions

The previous sections provide a consistent set of theoretical and experimental tools, which can be quantitatively applied to woven fabrics coated by hydrophobic formulations. The measurement of maps of roughness by profilometry allows us to sort fabrics and identify the ones which are most likely to exhibit high contact angles and low roll-off angles. These maps also give access to the projected fraction of wet fabric when in the superficially-wet state, and to the minimal image and droplet size from which measurements become independent of size. The maps can be separated into two components, arising from the weave pattern of the yarns, and from the packing of the fibers in yarns. It appears that the packing of the fibers in the yarns dominates by far the roughness of the samples. If
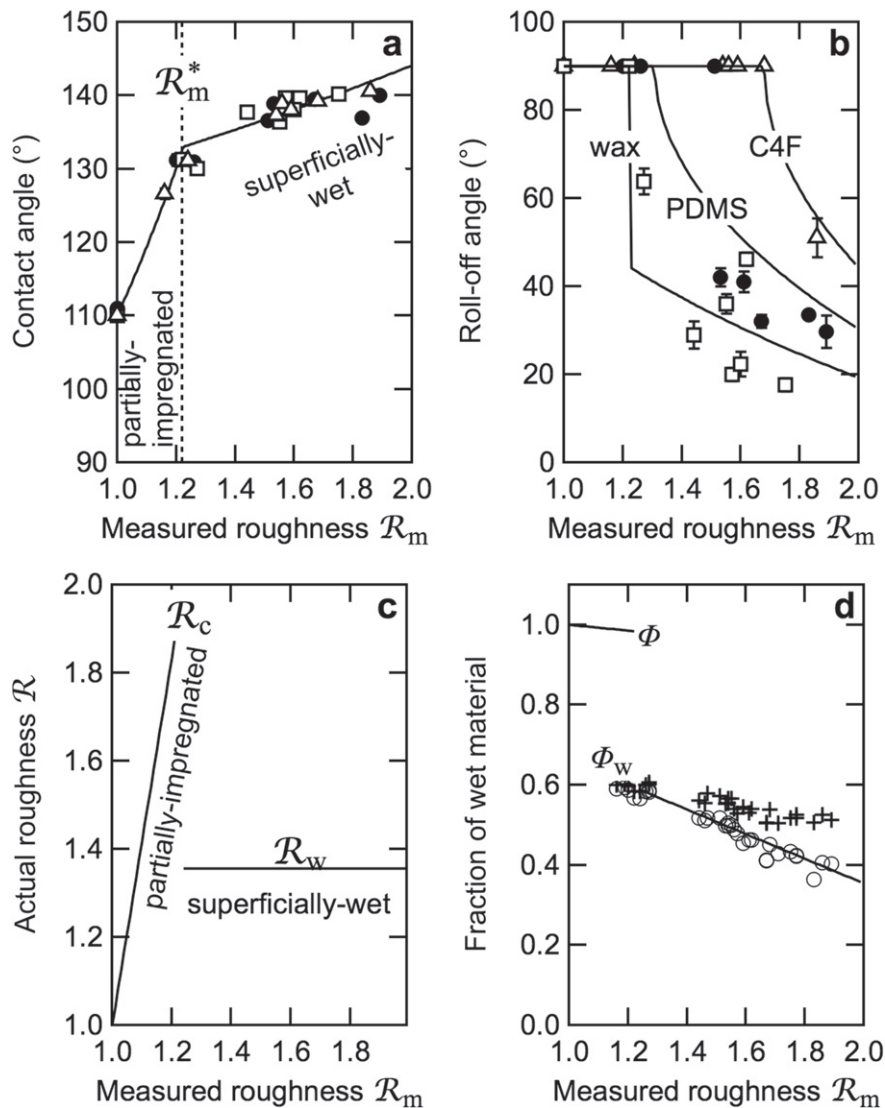
**Fig. 7.** Contact angles (a) and roll-off angles (b) of the coated fabrics of this study (in the absence of roll-off, $\theta_{ro}$ is set to 90°). Open squares indicate wax-coated samples, filled circles silicone-coated samples and open triangles perfluorobutyl-modified polyurethane-coated samples. The continuous lines in (a) and (b) are fits of Eqs. (2)/(4) and (8) to the contact and roll-off angle data, respectively, assuming the samples to be in a partially-impregnated state below a critical measured roughness ($\mathcal{R}_m^*$), and in the superficially-wet state above. The fitted actual roughness (Eqs. (32) and (34)) and fractions of wet solid (Eqs. (31) and (33)) are the continuous lines in panels (c) and (d), respectively. The symbols in panel (d) give the projected fraction of wet fabrics directly computed from the profilometry images using conditions (25), for theoretical flat contact angles $\theta_0$ of 110° (crosses) or 120° (circles).

the roughness needs to be increased, one should thus play with the packing of the fibers in the yarns rather than with the weave pattern.

Fabrics of measured roughness lower than a critical measured roughness $\mathcal{R}_m^*$ (1.22 for our standard conditions) are in a partially-impregnated state with a substantial pinning of the droplets on the surface and an absence of roll-off whatever the type of coating. Above this critical value, the fabrics enter the superficially-wet state, in which the water repellency becomes controlled by the amount of air trapped in the texture while the wet roughness remains constant. As the amount of trapped air increases in proportion to the measured roughness, rougher fabrics exhibit slightly higher water contact angles. Another factor which controls the amount of trapped air is the surface energy of the coating, or more precisely $\theta_0$: as Eq. (25) shows, $\phi_w$ decreases for more hydrophobic coatings (higher $\theta_0$), leading to higher contact angles as per Eq. (4).

However, being in the superficially-wet state is not by itself sufficient to ensure roll-off; the key control parameter for this property is the pinning parameter $\mu$, which is not a trivial parameter. There

has been a large body of work done on advancing and receding contact angles [29,30], which are related to the pinning parameter by Eq. (8); however, a comprehensive quantitative molecular model of $\mu$ is still to be developed [30,24]. Added to this is the fact that other, secondary parameters may also play a role in the roll-off; the role of a few protruding fibers which could act as pinning sites for a droplet is a particularly probable one. It would thus be erroneous to conclude from the present study that more fluffy fabrics would necessarily lead to smaller roll-off angles. Whereas fluffiness goes on a par with air trapping, it is likely that it would also increase pinning. This aspect was not studied here, and would be worthy of further investigation. Likewise, correlating fabric texture with water repellency for impacting droplet conditions is another topic for future research.

These results nevertheless suggest ways to improve water repellency. Increasing the roughness further might be done by nanostructuring the fibers (Eq. (29)), e.g., by adding nanoparticles to the coating formulations as done previously [31]; or by modifying the packing of fibers in yarns using specific spinning procedures. Developing

coatings of lower pinning parameter is certainly another promising route to follow, since results show that coatings of similar contact angle behave very differently with respect to water pinning, the fluorinated coating being worse than the silicone-based one, which is itself inferior to the wax-based one. In this respect, it is interesting to note that the two coatings of lower resistance to pinning are the ones for which environmental concerns are being voiced. The expected coming ban on short chain perfluoroalkanes [5] and the severe concerns related to the toxicity of cyclic silicone oligomers [32] should thus not be obstacles for the development of more environmentally-friendly fabrics displaying a good water repellency. The present study indicates that it is entirely possible to envision weaving a fabric in a way which favors water repellency and an easier rolling-off of water droplets on the fabric, without having to make use of substances of high environmental concern. We hope that this article will help contribute in reaching this goal.

## CRediT authorship contribution statement

**Alain M. Jonas:** Conceptualization, Methodology, Software, Formal analysis, Writing - original draft, Writing - review & editing, Supervision. **Ronggang Cai:** Validation, Investigation, Writing - review & editing. **Romain Vermeyen:** Methodology, Investigation. **Bernard Nysten:** Writing - review & editing, Supervision. **Myriam Vanneste:** Resources. **David De Smet:** Resources. **Karine Glinel:** Conceptualization, Writing - review & editing, Supervision.

## Data availability

Data will be made available on request.

## Declaration of competing interest

The authors declare that they have no known competing financial interests or personal relationships that could have appeared to influence the work reported in this paper.

## Acknowledgments

## Appendix A. Supplementary data

Supplementary Information is available (pdf document): Derivation of a general wetting equation for woven fabrics; Distribution of roughness of a fabric and minimal measurement sizes; Estimation of the projected fraction of wet solid for a fabric in the superficially-wet state; Separation of the roughness of a fabric in its two components (fiber packing in the yarns and weave pattern of the yarns); Profilometry images versus stylus scanning rate; Correlation functions of the local roughness for non-coated fabric surfaces; Variances of the distributions of roughness versus size; SEM images. Supplementary data to this article can be found online at https://doi.org/10.1016/j.matdes.2019.108389.

## References

[1] S. Pavlidou, R. Paul, Soil repellency and stain resistance through hydrophobic and oleophobic treatments, in: J.T. Williams (Ed.), "Waterproof and Water Repellent Textiles and Clothing", Woodhead Publishing, Duxford, 2018, pp. 73–88.

[2] X. Lim, The fluorine detectives, Nature 566 (2019) 26–29. https://doi.org/10.1038/d41586-019-00441-1.

[3] European Commission, Commission Regulation (EU) 2017|1000, Tech. rep., 2017, Brussels, Belgium. http://data.europa.eu/eli/reg/2017/1000/oj.

[4] C. Hogue, Governments endorse global PFOA ban, with some exemptions, Chem. Eng. News 97 (2019)5–5.

[5] S. Brendel, E. Fetter, C. Staude, L. Vierke, A. Biegel-Engler, Short-chain perfluoroalkyl acids: environmental concerns and a regulatory strategy under REACH, Environmen. Sci. Eur. 30 (1) (2018) 1–11. https://doi.org/10.1186/s12302-018-0134-4.

[6] R.N. Wenzel, Resistance of solid surfaces to wetting by water, Ind. Eng. Chem. 28 (8) (1936) 988–994. https://doi.org/10.1021/ie50320a024.

[7] A.B.D. Cassie, S. Baxter, Wettability of porous surfaces, Trans. Faraday Soc. 40 (1944) 546–551. https://doi.org/10.1039/tf9444000546.

[8] J. Bico, U. Thiele, D. Quéré, Wetting of textured surfaces, Coll. Surf. A 206 (2002) 41–46. https://doi.org/10.1016/S0927-7757(02)00061-4.

[9] A. Lafuma, D. Quéré, Superhydrophobic states, Nat. Mater. 2 (7) (2003) 457–460. https://doi.org/10.1038/nmat924.

[10] P.-G. de Gennes, F. Brochard-Wyart, D. Quéré, Capillarity and Wetting Phenomena. Drops, Bubbles, Pearls, Waves, Springer, New York, USA, 2004.

[11] A. Marmur, Wetting on hydrophobic rough surfaces: to be heterogeneous or not to be? Langmuir 19 (20) (2003) 8343–8348. https://doi.org/10.1021/la0344682.

[12] C. Yang, U. Tartaglino, B.N.J. Persson, Nanodroplets on rough hydrophilic and hydrophobic surfaces, Eur. Phys. J. E 25 (2) (2008) 139–152. https://doi.org/10.1140/epje/i2007-10271-7.

[13] A. Tuteja, W. Choi, G.H. McKinley, R.E. Cohen, M.F. Rubner, Design parameters for superhydrophobicity and superoleophobicity, MRS Bull. 33 (8) (2008) 752–758. https://doi.org/10.1557/mrs2008.161.

[14] H. Awada, B. Grignard, C. Jérôme, A. Vaillant, J. De Coninck, B. Nysten, A.M. Jonas, Correlation between superhydrophobicity and the power spectral density of randomly rough surfaces., Langmuir 26 (23) (2010) 17798–17803. https://doi.org/10.1021/la104282q.

[15] S.S. Chhatre, W. Choi, A. Tuteja, K.-C.K. Park, J.M. Mabry, G.H. McKinley, R.E. Cohen, Scale dependence of omniphobic mesh surfaces, Langmuir 26 (6) (2010) 4027–4035. https://doi.org/10.1021/la903489r.

[16] E. Bormashenko, Wetting transitions on biomimetic surfaces, Philosoph. Trans. Royal Soc. A: Math. Phys. Engineer. Sci. 368 (1929) (2010) 4695–4711. https://doi.org/10.1098/rsta.2010.0121.

[17] E. Bormashenko, General equation describing wetting of rough surfaces, J. Coll. Interface Sci. 360 (1) (2011) 317–319. https://doi.org/10.1016/j.jcis.2011.04.051.

[18] L. Afferrante, G. Carbone, Statistical theory of wetting of liquid drops on superhydrophobic randomly rough surfaces, Phys. Rev. E 92 (4). (2015) 042407–5. https://doi.org/10.1103/PhysRevE.92.042407.

[19] Q. Truong, N. Pomerantz, P. Yip, M. Sieber, J.M. Mabry, S.M. Ramirez, Pilot-scale coating of fabrics with fluorodecyl polyhedral oligomeric silsesquioxane/fluoroelastomer blends, Surface Innov. 2 (2) (2014) 79–93. https://doi.org/10.1680/si.13.00049.

[20] Q.T. Truong, N. Pomerantz, Military applications: development of superomniphobic coatings, textiles and surfaces, in: J.T. Williams (Ed.), "Waterproof and Water Repellent Textiles and Clothing", Woodhead Publishing, Duxford, 2018, pp. 473–531.

[21] S. Pan, R. Guo, M. Björnmalm, J.J. Richardson, L. Li, C. Peng, N. Bertleff-Zieschang, W. Xu, J. Jiang, F. Caruso, Coatings super-repellent to ultralow surface tension liquids, Nat. Phys. 17 (2018) 1040–1047. https://doi.org/10.1038/s41563-018-0178-2.

[22] S. Park, J. Kim, C.H. Park, Superhydrophobic textiles: review of theoretical definitions, fabrication and functional evaluation, J. Engineer. Fibers Fabrics 10 (4) (2015) 1–18.

[23] N. Pallas, Y. Harrison, An automated drop shape apparatus and the surface tension of pure water, Coll. Surfaces 43 (1990) 169–194. https://doi.org/10.1016/0166-6622(90)80287-E.

[24] J.W. Drelich, Contact angles: from past mistakes to new developments through liquid-solid adhesion measurements, Adv. Coll. Interface Sci. 267 (2019) 1–14. https://doi.org/10.1016/j.cis.2019.02.002.

[25] C.G.L. Furmidge, Studies at phase interfaces. I. The sliding of liquid drops on solid surfaces and a theory for spray retention, J. Coll. Interface Sci. 17 (1962) 309–324. https://doi.org/10.1016/0095-8522(62)90011-9.

[26] E.B. Dussan, V., On the ability of drops or bubbles to stick to non-horizontal surfaces of solids. Part 2. Small drops or bubbles having contact angles of arbitrary size, J. Fluid Mech. 151 (1985) 1–20. https://doi.org/10.1017/S0022112085000842.

[27] K.K. Varanasi, T. Deng, M.F. Hsu, N. Bhate, Design of superhydrophobic surfaces for optimum roll-off and droplet impact resistance, ASME International Mechanical Engineering Congress and Exposition, 2009, pp. 637–645. https://doi.org/10.1115/IMECE2008-67808.

[28] C.H. Edwards, Advanced Calculus of Several Variables, Academic Press, New York, USA, 1973.

[29] P.G. De Gennes, Wetting: statics and dynamics, Rev. Mod. Phys. 57 (3) (1985) 827–863. https://doi.org/10.1103/RevModPhys.57.827.

[30] H.B. Eral, D.J.C.M. 't Mannetje, J.M. Oh, Contact angle hysteresis: a review of fundamentals and applications, Coll. Polym. Sci. 291 (2) (2013) 247–260. https://doi.org/10.1007/s00396-012-2796-6.

[31] R. Cai, K. Glinel, D. De Smet, M. Vanneste, N. Mannu, B. Kartheuser, B. Nysten, A.M. Jonas, Environmentally friendly super-water-repellent fabrics prepared from water-based suspensions, ACS Appl. Mater. Interfaces 10 (18) (2018) 15346–15351. https://doi.org/10.1021/acsami.8b02707.

[32] European Chemicals Agency, Annex XV Restriction report - Proposal for a restriction - Octamethylcyclotetrasiloxane (D4), decamethylcyclopentasiloxane (D5), dodecamethylcyclohexasiloxane (D6), 2019, Helsinki, Finland.